Magnetic Resonance in Medicine 56:489–497 (2006)

Shear Wave Group Velocity Inversion in MR Elastography of Human Skeletal Muscle

Sebastian Papazoglou,[1] Jens Rump,[1] Jürgen Braun,[2] and Ingolf Sack[1]*

In vivo quantification of the anisotropic shear elasticity of soft tissue is an appealing objective of elastography techniques because elastic anisotropy can potentially provide specific information about structural alterations in diseased tissue. Here a method is introduced and applied to MR elastography (MRE) of skeletal muscle. With this method one can elucidate anisotropy by means of two shear moduli (one parallel and one perpendicular to the muscle fiber direction). The technique is based on group velocity inversion applied to bulk shear waves, which is achieved by an automatic analysis of wave-phase gradients on a spatiotemporal scale. The shear moduli are then accessed by analyzing the directional dependence of the shear wave speed using analytic expressions of group velocities in *k*-space, which are numerically mapped to real space. The method is demonstrated by MRE experiments on the biceps muscle of five volunteers, resulting in 5.5 ± 0.9 kPa and 29.3 ± 6.2 kPa ($P < 0.05$) for the medians of the perpendicular and parallel shear moduli, respectively. The proposed technique combines fast steady-state free precession (SSFP) MRE experiments and fully automated processing of anisotropic wave data, and is thus an interesting MRI modality for aiding clinical diagnosis. Magn Reson Med 56:489–497, 2006. © 2006 Wiley-Liss, Inc.

Key words: MR elastography; anisotropy; shear stiffness; bulk waves; biceps; balanced SSFP

MR elastography (MRE) is capable of monitoring bulk shear vibrations in soft biological tissues (1–4). The interest of physicians in imaging shear vibrations is based on the possibility of quantitatively testing in vivo stiffness variations, which would enable the detection of pathologies at an early stage. In MRE the sensitivity of wavelengths to elasticity changes is usually exploited to map elastic heterogeneities (5–9). In this way, local variations of wavelengths are analyzed in terms of local variations of the isotropic shear modulus using inversion algorithms. It is an inherent prerequisite of such isotropic inversion techniques that the waves propagate at equal speed through homogeneous elastic parts of the material. This does not hold true for anisotropic elastic material, such as skeletal muscle (10–12). Here the wave velocity generally depends on the direction of wave propagation, and shear wave images can thus display different wave numbers even in homogeneous elastic materials. This phenomenon is well known in crystal acoustics, where it is described using a vector of wave group velocity that is aligned with the direction of energy flux from the wave source (13,14). This contrasts with the scalar phase velocity, which denotes the wave speed along the wave front normals and which is usually deduced by isotropic inversion techniques. The purpose of this study was to develop a method for measuring group velocities in MRE of strongly anisotropic materials, such as skeletal muscles.

Extensive research in the field of muscle activity measurements by MRI underscore the important role of muscle MR in neurophysiologic research, diagnosis, and therapy (15–19). Muscle MRE (11,20–24) is developing into a straightforward technique for detecting several diseases that affect muscle elasticity, such as hypogonadism (25) and obstructive pulmonary disease (26). Thus it is increasingly important to correctly deduce all information about muscle elasticity from MRE shear wave patterns. As previously shown, applying isotropic inversion techniques to anisotropic wave images may yield misleading results (27). On the other hand, additional information about the mechanical properties of a material beyond scalar phase velocities can be gained by taking into account the directional dependency of the wave group velocity (28). Such an analysis would exploit the fact that the anisotropy of elasticity generates characteristic wave patterns, assuming 1) elastic homogeneity or shallow heterogeneity (on the scale of one wavelength), 2) a point source of the waves, and 3) non-reflecting boundary conditions. As previously shown, the special experimental conditions of in vivo muscle MRE apply in good approximation to these prerequisites (24). A group velocity inversion method would thus be applicable to MRE of skeletal muscles, and could reveal interesting information about the anisotropy of the mechanical properties of living muscle tissue.

In the following, a strategy for automatically detecting group velocities will be introduced in theory and demonstrated in MRE experiments of isotropic agarose gel and muscle biceps brachii from five volunteers. The new method can be outlined as follows:

1. The relationship between elastic coefficients and group velocity is derived in three dimensions for incompressible media. By this means, analytical expressions of wave speeds in *k*-space are received that model the shear wave-based elastography of biological tissues.
2. The analytical wave speed functions of *k* are numerically transformed into spatial dimensions, where they are automatically fitted to experimental group velocities by varying elastic coefficients. The experimental group velocities were previously determined by applying symmetry enhancement and automatic edge detection to phantom data and in vivo human biceps MRE data from five volunteers.

[1]Institute of Radiology, Charité-Universitätsmedizin Berlin, Berlin, Germany.
[2]Institute of Medical Informatics, Charité-Universitätsmedizin Berlin, Berlin, Germany.

Grant sponsor: German Science Foundation; Grant number: Sa-901/3.

*Correspondence to: Ingolf Sack, Ph.D., Institute of Radiology, Charité-Universitätsmedizin Berlin, Campus Mitte, Schumannstr. 20/21, 10117 Berlin, Germany. E-mail: ingolf.sack@charite.de

Received 1 September 2005; revised 12 May 2006; accepted 18 May 2006.
DOI 10.1002/mrm.20993
Published online 7 August 2006 in Wiley InterScience (www.interscience.wiley.com).

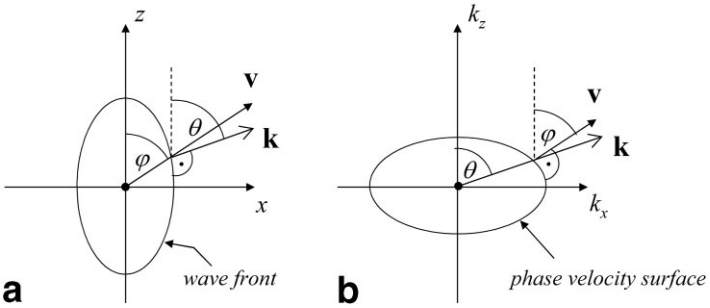

FIG. 1. Schematic 2D illustration of the directional relationship between group velocity **v** and wave vector **k** in the case of anisotropy. **a:** If waves emanate from a point source, their group velocity determines the wave front. **b:** In *k*-space, the inherent frequencies of a wave field are shown in relation to the phase velocity. Note: **k** and **v** are only parallel along their principal axes, which is fundamentally different from isotropic elasticity.

3. The potential influence of certain data acquisition and processing parameters on the results is investigated and discussed.

THEORY

Phase and Group Velocity of Waves in Anisotropic Media

In this study the basic principle of testing anisotropic elastic parameters by shear waves is the measurement of group velocities (13,14). This section summarizes the basic equations that enable a function of group velocities over space to be derived.

To start with, the basic wave equation of a displacement vector field **u** is given which models homogenous, anisotropic, and linearly elastic materials (applying Einstein's summation convention) (29):

$$\rho \ddot{u}_i - C_{ijkl}\frac{\partial^2 u_l}{\partial x_j \partial x_k} = 0. \quad [1]$$

where C_{ijkl} are the components of the elasticity tensor, and ρ denotes the density, which is 1 kg/l for agarose and 1.1 kg/l for muscle tissue. Using the plane wave solution

$$\mathbf{u} = \mathbf{U}e^{i(\mathbf{k}\mathbf{x}-\omega t)} \quad [2]$$

with **U**, **k,** and **x** as the vectors of initial polarization, wave numbers, and position, respectively, directly yields Christoffel's equation:

$$(C_{ijkl}n_j n_k - \rho c^2 \delta_{il})U_l = 0. \quad [3]$$

where n_i are the components of the wave normal ($\mathbf{n} = \mathbf{k}/|\mathbf{k}|$,), c is the scalar phase velocity ($c = \omega/|\mathbf{k}|$), and δ_{il} is Kronecker's delta. Nontrivial solutions for the polarization vector **U** exist only for those phase velocities c that satisfy the characteristic equation

$$\det(C_{ijkl}n_j n_k - \rho c^2 \delta_{il}) = 0. \quad [4]$$

This equation is of degree d with respect to c^2, where d is the spatial dimension. Consequently, there are three different modes in 3D space (indexed hereafter by capital subscripts) for any given **n**. These modes are characterized by the orientation of their polarization vector **U** with respect to **n** as quasi-longitudinal (*L*) or quasi-transverse, one being a slow transverse (*ST*) mode and the other a fast transverse (*FT*) one. The term "quasi" is used because in an anisotropic medium **U** and **n** do not have to be strictly parallel or perpendicular to each other for every direction of wave propagation **n**. The mode showing the smallest angle between **U** and **n** is commonly referred to as the quasi-longitudinal mode. Any wave propagating in an anisotropic medium can be considered to be a superposition of plane waves according to Eq. [2], which shows different phase velocities depending on the direction of **n** (Eq. [4]). In particular, a small volume fraction of the wave front is a superposition of plane waves that travel in slightly different directions at slightly different phase velocities. As a result this fraction or group of plane waves as a whole travels at a common speed, called the group velocity (13):

$$\mathbf{v}_M = \frac{\partial c_M}{\partial \mathbf{n}}. \quad [5]$$

If there is a point source of the waves, the group velocity is directly accessible. It is the speed at which the wave propagates along the rays outward from the source. Deviations of the directions of **n** and **v** indicate anisotropy. Figure 1 shows a sketch of the phase velocity surface and wave front projected onto the x_1-x_3-plane (labeled in the following as x and z, respectively) that is considered to be the image plane in the MRE experiments. Here, two angles θ and φ describe the directions of **n** and **v**, respectively. While the function $\mathbf{v}_M(\varphi)$ is the experimentally measured quantity, $\mathbf{v}_M(\theta)$ is available from theory (Eqs. [4] and [5]). For an inversion based on group velocity measurements, it is therefore necessary to relate the two angles. However, to our knowledge, it is not possible to give analytical expressions for all modes $\mathbf{v}_M(\varphi)$. On the other hand, it is feasible to derive φ using the components of any group velocity mode, as shown in Fig. 1a,

$$\varphi = \arctan\left(\frac{V_1}{V_3}\right), \quad [6]$$

and to numerically plot $\mathbf{v}_M(\varphi)$. Changing the elastic coefficients C_{ijkl} allows the fitting of experimental group velocities to single wave modes in spatial coordinates. The dependency of the phase and group velocities from these elastic constants, which applies to shear-wave elastography, is derived as described below.

Shear Waves in Transverse Isotropic Elastic and Incompressible Materials

Henceforth the elasticity of skeletal muscle is assumed to be essentially transversely isotropic. Thus, the plane of

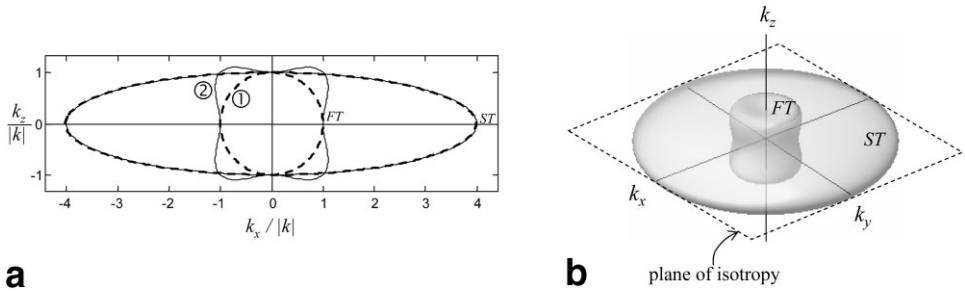

FIG. 2. **a:** Phase velocity surfaces $\rho c_M^2 = 1$ kPa according to Eq. [8] in normalized *k*-space plotted for two elastic scenarios: $\mu_{12} = 1/16$ kPa, $\mu_{13} = 1$ kPa, $E_3/E_1 = 16$ (case 1, dashed graphs), $E_3/E_1 = 8$ (case 2, solid graphs; unit density of 1 kg/l). The concave curvature of the *FT*-mode of case 2 yields caustics of spatial waves. **b:** 3D representation of case 2 in a.

symmetry is spanned by the *x*- and *z*-axes, which define the corresponding axial elastic moduli (Young's moduli) $E_1 = E_2$ and E_3. The principal axis of symmetry (*z*) is assumed to be aligned with the long axis of the muscle so that it is parallel to the muscle fibers (12,24,27,30).

The transverse symmetry reduces the number of independent elastic constants to five. Further simplification can be gained in shear-wave-based elastography if the effects of compressibility are neglected. Since most biological materials are nearly incompressible, such effects give rise to longitudinal waves that travel orders of magnitude faster than shear waves. Therefore, high-pass filtering would suppress the displacement of the longitudinal wave mode that varies only slightly in the far-field range of the source (31).

Assuming incompressibility, the elasticity tensor **C** can be expressed in the limit of Poisson's ratio $v_{31} = 1/2$ (denoted by the Greek "nu" in contrast to the italic "*v*" for velocities):

$$C_{1111} = \lim_{v_{31}\to 0.5} \frac{(\mathrm{E}_3 - \mathrm{v}_{31}^2\mathrm{E}_1)\mathrm{E}_3}{(2\mathrm{v}_{31}-1)(\mathrm{v}_{31}\mathrm{E}_1 - 2\mathrm{E}_3)\mathrm{v}_{31}}$$

$$C_{1122} = \lim_{v_{31}\to 0.5} \frac{(E_3 - v_{31}E_1 + v_{31}^2E_1)E_3}{(2v_{31}-1)(v_{31}E_1 - 2E_3)v_{31}}$$

$$C_{1133} = C_{2233} = C_{3333} = \lim_{v_{31}\to 0.5} \frac{E_3}{1-2v_{31}}$$

$$C_{1212} = \mu_{12} = \frac{E_1E_3}{4E_3 - E_1}$$

$$C_{1313} = C_{2323} = \mu_{13} \qquad [7]$$

The dependent ratios v_{13} and v_{12} are derived in Appendix A. Apart from the shear moduli μ_{12} and μ_{13}, all elements of the elasticity tensor diverge. Inserting the algebraic expressions of C_{ijkl} into Eq. [4] and solving for c^2 yields three eigenmodes, including one diverging longitudinal wave mode that is discarded from further analysis. The other two modes are obtained using de l'Hôpital's rule:

$$\rho c_{ST}^2 = \mu_{12}(n_1^2 + n_2^2) + \mu_{13}n_3^2$$

$$\rho c_{FT}^2 = 4\left(\mu_{13} - \mu_{12}\frac{E_3}{E_1}\right)\left(\frac{n_3^4}{\mathbf{n}^2} - n_3^2\right) + \mu_{13}\mathbf{n}^2 \qquad [8]$$

Figure 2 demonstrates the shape of phase velocity contours of *ST*- and *FT*-mode for two elastic cases that deviate solely by the ratio of the Young's moduli E_3/E_1. Since the *ST*-mode controls pure out-of-plane displacement in the case of transverse isotropy, c_{ST} in Eq. [8] also applies to compressible media. Its shape is described by an ellipsoid whose axes are determined by μ_{12} and μ_{13} (14). In contrast, c_{FT} additionally depends on the ratio E_3/E_1, resulting in more complex wave patterns for $E_3/E_1 \neq \mu_{13}/\mu_{12}$. Since the *FT*-mode also describes in-plane motions, the given expression applies only to incompressible materials.

The displacement field in real space resulting from harmonic transducer motions can be calculated as described in Appendix B. Accordingly, Fig. 3 shows the displacement vector components $u_1(x_1,0,x_3)$, $u_2(x_1,0,x_3)$, $u_3(x_1,0,x_3)$ with excitation along *x*, *y*, and *z*, respectively, for the elastic scenarios corresponding to Fig. 2. It is apparent that μ_{12} and μ_{13} are simultaneously accessible by out-of-plane waves, while the ratio E_3/E_1 can only be estimated by in-plane deflections.

To analyze the experiments, it is necessary to know whether the observed waves in MRE are due to the *ST*-mode, the *FT*-mode, or a superposition of both wave modes. Fortunately, MRE allows the encoding and, in some cases, also the excitation of single components of **u** with an arbitrary image slice position. We observed pure *ST*-waves in our experiments, since only motions perpendicular to the image plane were excited and encoded. In general, the experimental setup is chosen in such a way as to avoid a superposition of *ST*- and *FT*-wave modes. Thus the image plane must be aligned with the principal axes of the wave field, which in turn will be polarized along a principal axis of the elasticity tensor. *ST*- and *FT*-waves are then separately visible so that $\mathbf{v}_M(\varphi)$ can be analyzed by the corresponding c_M in Eq. [8]. In this paper the analysis of group velocities $\mathbf{v}(\varphi)$ (assignable to an arbitrary wave mode *M*) is based on rays $\mathbf{r}(\varphi)$ (with length *r*) emanating from the apparent point source of the waves. Along such rays, the wavelength λ varies with ι due to the anisotropy of the elasticity.

MATERIALS AND METHODS

MRE Experiments

MR experiments were performed on a 1.5 T scanner (Magnetom Sonata; Siemens, Erlangen, Germany). For image

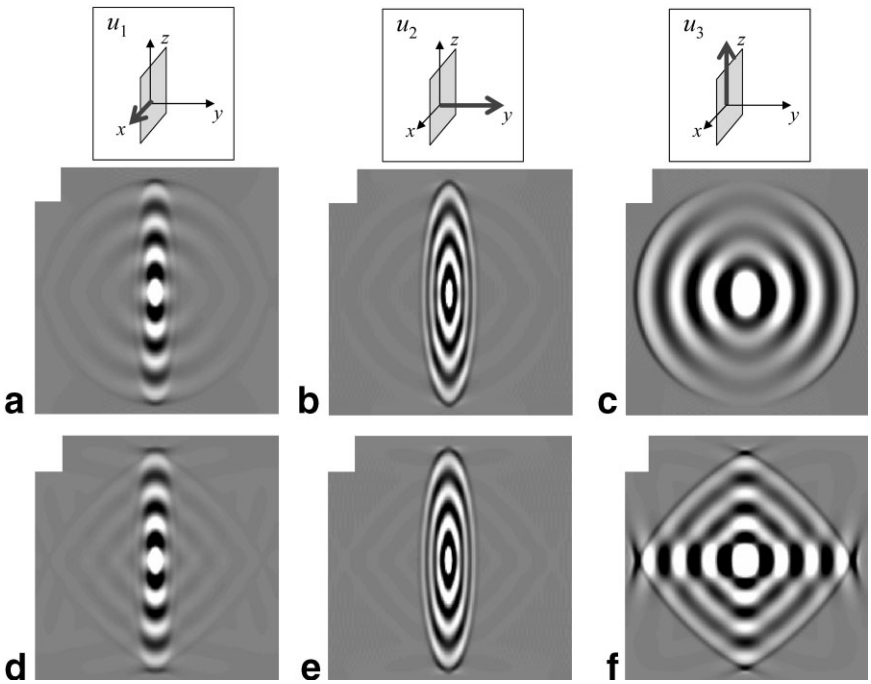

FIG. 3. Calculated wave images using Eq. [19] (see Appendix B). The plane of projection and the polarization of **u** (which is parallel to the initial polarization **U**) are symbolized in the pictograms at the first row. The elastic parameters correspond to cases 1 (**a–c**) and 2 (**d–f**) in Fig. 2a. The image planes are aligned with the principal axis system so that *ST*- and *FT*-wave modes can be seen separately. The out-of-plane deflection given in b and e is governed by c_{ST}, while transverse waves travel perpendicular to this plane with c_{FT} (see Eq. [8]).

acquisition a modified balanced steady-state free precession (*b*-SSFP) sequence incorporating trapezoidal oscillating motion-encoding gradients (MEG) in slice-select direction was used. As described in Ref. 32, the vibration frequency was chosen to be equal to n_v/TR (with integer n_v) to avoid image artifacts in the phase-encoding direction. The image acquisition parameters were as follows: FOV, matrix size, slice thickness, and flip angle = 150 mm, 128 × 128, 5 mm, and 65°, respectively. The elastography parameters of vibration frequency ($\omega/(2\pi)$), number of vibration cycles (n_v), MEG frequency, number of MEG periods, and MEG amplitude were adjusted to be 205 Hz, 3, 205 Hz, 2, and 35 mT/m in phantom studies, and 75–126 Hz, 1, 100–200 Hz, 1, and 35 mT/m in volunteer studies, respectively.

Shear vibrations were introduced to the phantom using an electromechanical actuator (33) whose transducer rod plugged a few millimeters into the gel. In vivo experiments were performed on five healthy male volunteers (mean age = 35 years). To investigate the biceps, an electromechanical rocker unit was attached to the distal tendon (11). The volunteers described their subjective feelings during mechanical muscle stimulation as being similar to vibrations from an electric razor. The direction of transducer motions was approximately in the anterior–posterior (A-P) direction. In our standard protocol, motion sensitization was parallel to the principal direction of the vibration (y) and perpendicular to the image plane (x - z) (Fig. 4). Twenty wave images were acquired by toggling the direction of motion sensitization to produce 10 phase difference

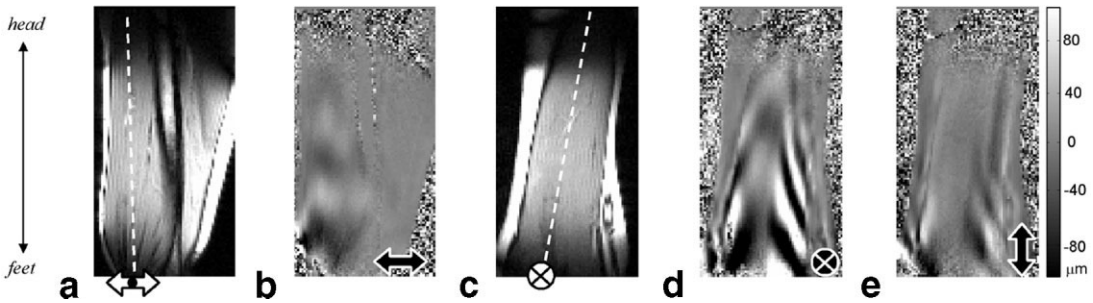

FIG. 4. MRE of the human biceps with mechanical excitation of 99 Hz. The magnitude images (**a** and **c**) display the anatomical contrast of the adjacent phase-difference images (**b**, **d**, and **e**). The perpendicular image planes are aligned with the long axis of the biceps, which represents the mutual image axis (dashed graphs). White symbols indicate the direction and the source of in-plane (⇔) and out-of-plane (⊗) vibrations. The actuator attached to the distal tendon induced mainly unidirectional up-and-down vibrations. Correspondingly, the black symbols indicate the direction of motion sensitization and thus the polarization of the waves. a: Image slice parallel to the vibration direction with demarcation (dashed line) of the position of the perpendicular images c, d, and e. b: Transverse in-plane waves corresponding to the *FT*-mode (cf., Fig. 3a and d). c: Image plane through the origin of the waves perpendicular to the motion. The dashed line indicates the image plane of a and b. d: Out-of-plane waves parallel to the direction of the transducer vibrations ($u_2(x,z,t)$). This setup was applied in volunteer studies to acquire pure *ST*-wave images. e: In-plane motions encoded perpendicular to the major direction of wave excitation. Since an excitation of waves parallel to the tendon was experimentally not feasible, only minor fractions of the waves arise in the vicinity of the muscle boundaries.

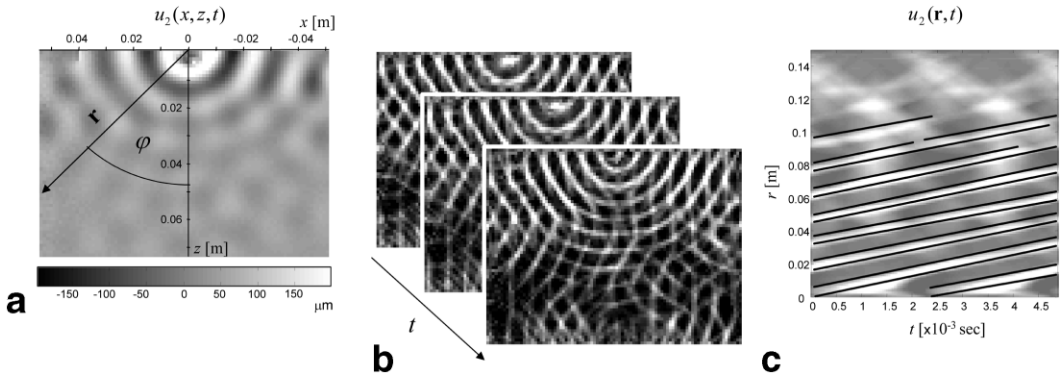

FIG. 5. **a:** Experimental MRE wave image of agarose subjected to 205 Hz mechanical excitation. For determination of group velocities **v**(φ) the vector **r** is rotated with φ. **b:** Phase symmetry-enhanced contrast images of a with additional temporal resolution to demonstrate the propagation of wave fronts. **c:** Symmetry enhanced wave propagation of a 1D-spatial profile corresponding to the vector **r** in a with φ = 45°. Lines of constant phase (solid lines) were automatically found using edge detection. The algorithm was adjusted to ignore fractional wave fronts due to scattering at boundaries (here at $r > 0.11$ m). The slopes of the curves represent **v**(φ = 45°).

wave images $u_2(x,z,t)$ by complex image subtraction (34). A delay between the onset of the mechanical excitation and the start of motion encoding was increased 10 times to increment ωt from 0 to 2π. The total measure time was 50 s.

The reproducibility of the method was validated on the biceps muscle of volunteer 2. Eight MRE studies with mechanical vibration frequencies from 75 to 118 Hz were performed on five different days.

Automatic Determination of Experimental Group Velocities

To analyze group velocities, we fed the segmented and unwrapped phase difference data into an inversion program written in Matlab (The MathWorks, Inc., Natick, MA, USA) based on the following steps:

1. Manual demarcation of the coordinate system and the lengths of **r** (Fig. 5a).
2. Phase contrast enhancement based on Ref. 35 (Fig. 5b).
3. Interpolation of *r*-*t*-images ($u_2(\mathbf{r},t)$) corresponding to **r**(φ) with variation of φ in increments of 5° (Fig. 5c). To avoid boundary effects, φ was changed between either ±80° or ±60° for agarose and muscle tissue, respectively.
4. Automatic recognition of wave slopes (**v**(φ)) in $u_2(\mathbf{r},t)$ (see Fig. 5c) by an edge detection algorithm based on the Canny method in Matlab. To minimize boundary artifacts φ was varied between ±80° for agarose and ±60° for the biceps.
5. Fit of the experiments: The analytical solution of Eq. [5] is used with variable combinations of μ_{12} and μ_{13} to calculate $\mathbf{v}_{ST}(\theta)$. Then, $\varphi(\theta)$ is calculated using Eq. [6] to map $\mathbf{v}_{ST}(\theta)$ vs. $\varphi(\theta)$ and determine the variation between experimental and calculated curves, which is defined here as the mean of $|\mathbf{v}(\varphi) - \mathbf{v}_{ST}(\varphi(\theta))|$ normalized by the standard deviation (SD) of the experimental data. This procedure was repeated 100 times from 0.5 to 20 kPa with independently varying μ_{12} and μ_{13}. The resulting variations were stored in memory as functions of μ_{12} and μ_{13}. The shear moduli at the global minimum of all variations were taken as the final results. The value of the minimum itself was used as error tolerance of the wave speeds if no multiple experiments were performed (as in volunteer 2).

This routine was tried with $r = \lambda$ on synthetic circular waves with $\bar{v} \equiv (v_1 + v_3)/2 = 2.87$ m/s, and on experimental circular waves observed in agarose. The stability against a decrease of SNR was investigated by adding noise to both synthetic and experimental waves.

In muscle the *x*-*z*-coordinates were aligned corresponding to the direction of largest wave lengths, as demonstrated in Fig. 6. The length of **r** was limited by the size of the region of interest (ROI), yielding $r = 0.13$ m, 0.134 m, 0.11 m, 0.107 m, and 0.132 m for volunteers 1–5, respectively.

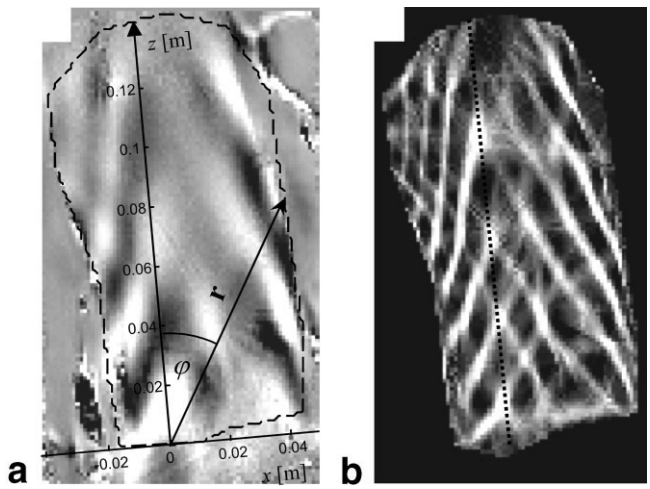

FIG. 6. Wave data $u_2(x,z,t)$ of volunteer 1. **a:** Phase contrast MRE wave image acquired with 126.3 Hz mechanical actuation. The length of **r** was constrained by the boundaries of the ROI (dashed line). **b:** Symmetry-enhanced wave image of a. The principal muscle axis (indicated as dotted line) is clearly distinguishable through tapered waves.

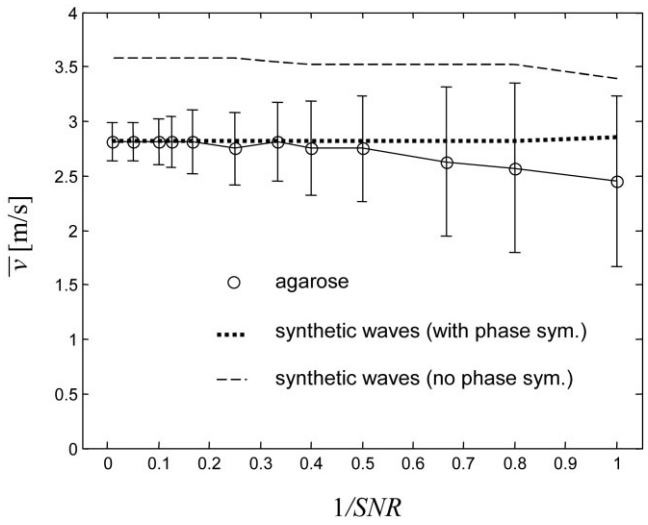

FIG. 7. Application of the wave inversion program to synthetic isotropic waves and phantom experiments modified by added noise. In simulations $\bar{v}$ (i.e., the mean of v_1 and v_3) was 2.87 m/s for reproducing phantom experiments at their initial SNR of 82. Edge detection with synthetic data was performed with and without phase symmetry enhancement ($r = \lambda$ for all data).

RESULTS

Equation [8] provides an analytical relation between the elastic moduli and phase velocity surface, showing that μ_{12}, μ_{13}, and the ratio E_3/E_1 are the only elastic parameters that are relevant for group velocity inversion applied to incompressible, transversely isotropic media. Interestingly, it is not possible to deduce all three elastic parameters from a single component of **u**. This is illustrated by Fig. 3, which shows the dependency of the shear wave form on distinct functions of phase velocity in *k*-space (Fig. 2). These simulations reproduce the experimental scenarios shown in Fig. 4, which reveal that only the *ST*-waves on the biceps bear significant information about the elastic anisotropy of the material**.** In contrast, *FT*-waves are either limited due to muscle boundaries or are too weakly excited by the conventional actuator that is based on a rocker design. Consequently, the setup of volunteer experiments was chosen to obtain waves correspondingly to Fig. 4d.

Figure 7 demonstrates the effect of noise on the inversion technique. The variation in the fit of the synthetic data was at maximum ± 0.4 m/s. Omitting the phase-symmetry enhancement prior to the edge detection resulted in an overestimation of the wave speeds of about 30%. This deviation decreased with an increasing length of the rays. An *r* of approximately 4λ yielded correct wave speeds even without phase symmetry enhancement. The wave speed in agarose was found to be 2.87 ± 0.19 m/s at the initial SNR of 82. Decreasing SNR leads to an about 15% underestimation of $v(\varphi)$ at SNR = 1. Synchronously, the error tolerances increase up to 300%, which indicates increased scattering of the detected wave slopes, although their mean remains largely constant.

Figure 8 illustrates group velocity inversion on the human biceps of five volunteers in comparison to isotropic waves acquired in agarose. The group velocities of muscle

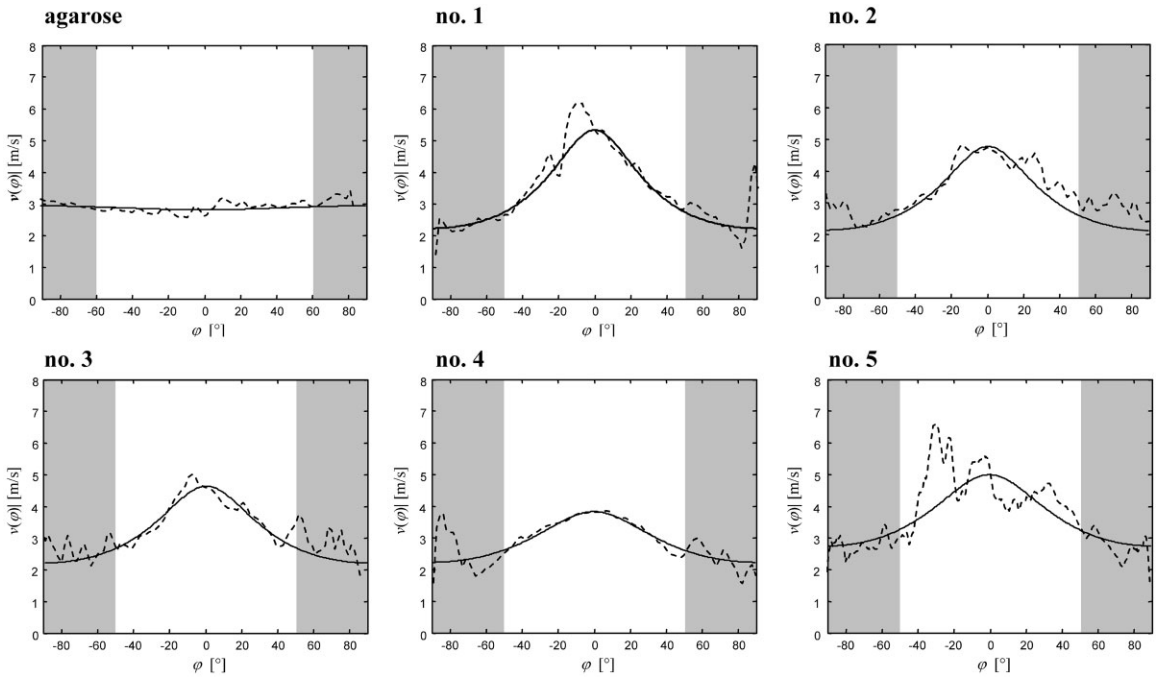

FIG. 8. Experimental magnitude of group velocities $v(\varphi) = |\mathbf{v}(\varphi)|$ in agarose and human biceps of volunteers 1–5 (corresponding to the labels above the graphs). Although φ was varied between ±90° a constricted range was used to determine the minimum variation between experiment (dashed graphs) and simulated $\mathbf{v}_{ST}(\varphi)$ (solid curves). The considered φ range (white area) was ±80° for agarose and ±60° in muscle experiments, which takes into account that the ROI is shorter in *x* than in *z* (see Fig. 7a). The values of μ_{12} and μ_{13} used to fit the data are listed in Table 1.

Table 1
Shear Wave Velocities of the Slow Transverse (*ST*) Wave Mode (v_1, v_3) and Anisotropic Shear Moduli (μ_{12}, μ_{13}) of Agarose and the Biceps Muscle of Volunteers 1 to 5*

	Agarose	1	2[a]	3	4	5	1–5[b]
v_1 [m/s]	2.93 (0.19)	2.22 (0.23)	2.27 (0.19)	2.21 (0.36)	2.22 (0.25)	2.69 (0.44)	2.22 (0.18)
v_3 [m/s]	2.81 (0.19)	5.32 (0.23)	5.28 (0.45)	4.62 (0.36)	3.82 (0.25)	5.13 (0.44)	5.13 (0.55)
v_3/v_1	0.97 (0.13)	2.43 (0.35)	2.36 (0.4)	2.18 (0.52)	1.75 (0.31)	1.99 (0.49)	2.35 (0.44)
μ_{12} [kPa]	9.5 (1.22)	5.48 (1.1)	5.69 (0.95)	5.51 (1.75)	5.5 (1.2)	8.18 (2.6)	5.46 (0.88)
μ_{13} [kPa]	8.74 (1.17)	31.21 (2.64)	30.89 (5.23)	23.66 (3.67)	16.11 (2.07)	29.21 (4.96)	29.28 (6.21)
μ_{13}/μ_{12}	0.95 (0.25)	6.03 (1.69)	5.74 (1.87)	5.02 (2.26)	3.17 (1.07)	4.19 (1.94)	5.7 (2.06)

*The variations between simulation and experiments (see Materials and Methods) are given in parentheses. In muscle tissue, μ_{12} corresponds to the shear modulus perpendicular to the muscle fibers (within the plane of isotropy), while μ_{13} represents the shear stiffness parallel to the fibers.
[a]In this column, the tolerances correspond to the standard deviation between eight experiments performed on five different days with variable mechanical excitation frequencies from 75 to 118 Hz.
[b]The median of all volunteer studies with 95% confidence intervals.

tissue clearly differ from isotropic wave speeds by the shape of their functions over φ. While the wave speed vector **v** of an isotropic elastic material is represented by a circle with constant radius $v(\varphi)$, in muscle tissue $v(\varphi)$ changes elliptically with v_3 greater than 2.86 ($\pm$ 0.41) v_1 (interindividual median). The group velocities and corresponding shear moduli used to fit the experiments are listed in Table 1.

We found no significant correlation between shear wave speed and vibration frequency. The limit of viscosity that would cause significant wave dispersion in the biceps can be estimated by assuming Voigt's relation between wave speed dispersion and excitation frequency in a viscous body. Such maximum viscosity is approximately given by 3.5 $\pm$ 1.0 Pas. Since we found no dispersion in our experiments, we assumed a viscosity below this value and thus calculated all shear moduli in Table 1 in the absence of viscosity, which resulted in an error below the experimental accuracy.

DISCUSSION AND CONCLUSIONS

Our data demonstrate the capability of group velocity inversion to measure anisotropic shear moduli in MRE. In this new approach, anisotropic elastic parameters are derived by means of the full directional dependency of group velocities over φ, rather than by measuring scalar quantities along axial profiles.

This considerably improves the feasibility of anisotropic MRE of skeletal muscle, since a direct evaluation of wave speeds at axial profiles is often hampered by the limited spatial resolution in the short-axis direction of the muscle (24). Using group velocity inversion, it is possible to adapt the spatial sector of wave inversion to a boundary-free ROI. This can be particularly important for evaluating MRE experiments of thin muscle layers or less separated muscle groups (21–23,36). As Fig. 8 illustrates, the anisotropy of wave propagation was analyzed within a sector of $\pm 60°$ relative to the principal axis of the biceps. As a result, the deduced shear modulus μ_{12} of all investigated biceps was confined by a narrow confidence interval of 0.88 kPa with a median of 5.46 kPa. Since this elastic parameter is related to the short axis of the biceps, it indicates the stability of the method against boundary effects.

Few in vivo data regarding shear moduli perpendicular to skeletal muscle fibers are available from US elastography or MRE studies. These data also vary considerably. Although values in the range of 0.92 kPa were found by transient US elastography (37), previous MRE studies revealed much higher values of 16 kPa (10) and 14.8 kPa (38). A previous analysis of anisotropic wave forms yielded values between 3.4 kPa and 8 kPa (24), which is similar to the quantities measured by group velocity inversion in the present study. However, that analysis revealed much higher values of μ_{13} (~54 kPa), with a ratio μ_{13}/μ_{12} of approximately 16. Such a ratio fits with anisotropic shear moduli determined in transient US elastography (12). In contrast, the present study revealed a maximum ratio of 6.03 $\pm$ 1.69 (volunteer 1). The difference may be due to the elliptical wave form predicted by the *ST* mode that was not seen in the MRE wave data of the biceps. It was previously shown (24) that straight waves emerging as "*V*-waves" result from a certain combination of three elastic parameters of a plate model, which does not support the existence of bulk shear waves in muscle. The proposed elastic model is the simplest 3D bulk shear wave model for transverse isotropic solids. The absence of reflecting boundaries assumes the absence of shear wave scattering and wave mode conversions. These processes in combination with surface effects surely influence the observed wave shape. Despite this weakness of the model used to explain the correct *V*-wave shape, it is feasible to fit $v(\varphi)$ curves as demonstrated by Fig. 8. The obtained variations for v_1 and v_3 are reasonably low with regard to inverse problems in shear-wave-based elastography (39).

The proposed phase gradient method for automatically detecting wave velocities is a robust technique that provides reproducible results even for noisy data with low wave numbers. For such data the enhancement of wave contrast based on symmetry recognition supports an automatic fit of the wave fronts. However, when r covers at least three to four wavelengths, the applied edge detection robustly recognizes wave fronts even without prior symmetry enhancement.

It is important to note that group velocity inversion requires the image slice to be aligned with the focal wave source. This prerequisite fails if bundles of muscle fibers cross the image plane along a bent principal axis of the muscle so that the waves are guided through-plane. In that case, geometrical biases would result in an overestimation of the deduced wave speeds. Such biases can be mitigated by the special property of straight *V*-waves characterized by self-repeating patterns along the principal axis of the muscle (24). This hypothesis is supported by an analysis of position-dependent group velocities with the origin of **r** shifted away from the wave source (data not shown). This point should be further validated in ongoing work. Thus far, aligning an image slice with two principal axes of the elastic tensor that combine the focal origin of the waves is the most general prerequisite for successfully applying group velocity inversion.

In summary, the determination of anisotropic elastic moduli by group velocity inversion is straightforward if the spatial-temporal propagation of focally excited shear waves is measured within an image plane that captures two principal axes of the tissue. The proposed elasticity model is able to fit wave speeds detected along rays even though it cannot reproduce typical *V*-shaped shear wave patterns in the biceps revealed by MRE. Although this study focused on skeletal muscle, the described strategy of group velocity inversion is principally applicable to other types of tissue if the given experimental prerequisites are fulfilled.

APPENDIX A

To derive the elasticity tensor of an incompressible material, we first define the trace of the strain tensor $\boldsymbol{\epsilon}$ to be a small number δ that is close to zero:

$$\varepsilon_{ii} = \delta. \qquad [9]$$

Then, for the Poisson's ratios, $v_{ij} = \varepsilon_{jj}/\varepsilon_{ii}$ (with $i \neq j$, no summation over repeating indices) follows

$$v_{ij} + v_{ik} = (1 - \zeta_{ii}) \quad \text{with } \zeta_{ii} = \frac{\delta}{\varepsilon_{ii}}, \qquad [10]$$

which allows us to express all Poisson's ratios as function of only one ζ_{ii}. Thus, with respect to the principal axis z, we obtain

$$v_{31} = v_{13}\frac{E_3}{E_1} = \frac{1}{2}(1 - \zeta_{33}). \qquad [11]$$

The compressibility ratio of the isotropy plane is then given by

$$\zeta_{11} = -v_{13}\zeta_{33} = \frac{1}{2}\frac{E_1}{E_3}(\zeta_{33}^2 - \zeta_{33}), \qquad [12]$$

yielding

$$v_{12} = 1 + \frac{E_1}{E_3}\left(\zeta_{33} - \frac{1}{2}\zeta_{33}{}^2 - \frac{1}{2}\right). \qquad [13]$$

In the limit of incompressibility, v_{31} and v_{12} are given as

$$\lim_{\zeta_{33}\to 0} v_{31} = \frac{1}{2} \qquad [14]$$

$$\lim_{\zeta_{33}\to 0} v_{12} = 1 - \frac{1}{2}\frac{E_1}{E_3}.$$

APPENDIX B

The solution for specific initial value problems in the equation of motion (Eq. [1]) is demonstrated by assuming an initial condition $\mathbf{u}_0 = [\delta(\mathbf{x}),0,0]^T$ and $\dot{\mathbf{u}}_0 = 0$, which reads in *k*-space:

$$\mathbf{w}_0 = [1,0,0]^T \quad \text{and} \quad \dot{\mathbf{w}}_0 = 0. \qquad [15]$$

Defining

$$V_{ij} = (U^{-1})_{ij} \qquad [16]$$

where **U** is the matrix whose columns are the eigenvectors determined from Eq. [3]. after solving Eq. [4] for the eigenvalues ($\omega_i = c_i|\mathbf{k}|$), one finds the solution of the initial value problem first in the eigensystem:

$$\bar{w}_i = V_{i1}\cos(\omega_i t) \qquad [17]$$

and finally in the initial frame:

$$w_l = U_{li}\bar{w}_i = U_{li}V_{i1}\cos(\omega_i t). \qquad [18]$$

This is the solution of the Fourier-transformed equation of motion (Eq. [1]) subject to the initial condition Eq. [18]. The solution in real space is finally obtained by inverse Fourier transform in three dimensions:

$$u_l(\mathbf{x},t) = \frac{1}{(2\pi)^3}\int_{-\infty}^{\infty} dk_1 \int_{-\infty}^{\infty} dk_2 \int_{-\infty}^{\infty} dk_3 U_{li}V_{i1}\cos(\omega_i t)e^{i(k_j x_j)}. \qquad [19]$$

This solution corresponds to a transient excitation at the origin of the coordinate system at time $t = 0$. The response to a harmonic steady-state excitation can now be obtained by convoluting Eq. [19] with a harmonic source.

REFERENCES

1. Muthupillai R, Lomas DJ, Rossman PJ, Greenleaf JF, Manduca A, Ehman RL. Magnetic resonance elastography by direct visualization of propagating acoustic strain waves. Science 1995;269:1854–1857.
2. Plewes DB, Betty I, Urchuk SN, Soutar I. Visualizing tissue compliance with MR imaging. J Magn Reson Imaging 1995;5:733–738.
3. Muthupillai R, Rossman PJ, Lomas DJ, Greenleaf JF, Riederer SJ, Ehman RL. Magnetic resonance imaging of transverse acoustic strain waves. Magn Reson Med 1996;36:266–274.
4. Lewa CJ, De Certaines JD. Viscoelastic property detection by elastic displacement NMR measurements. J Magn Reson Imaging 1996;6:652–656.

5. Van Houten EE, Paulsen KD, Miga MI, Kennedy FE, Weaver JB. An overlapping subzone technique for MR-based elastic property reconstruction. Magn Reson Med 1999;42:779–786.
6. Sinkus R, Lorenzen J, Schrader D, Lorenzen M, Dargatz M, Holz D. High-resolution tensor MR elastography for breast tumour detection. Phys Med Biol 2000;45:1649–1664.
7. Oliphant TE, Manduca A, Ehman RL, Greenleaf JF. Complex-valued stiffness reconstruction for magnetic resonance elastography by algebraic inversion of the differential equation. Magn Reson Med 2001;45: 299–310.
8. Braun J, Buntkowsky G, Bernarding J, Tolxdorff T, Sack I. Simulation and analysis of magnetic resonance elastography wave images using coupled harmonic oscillators and Gaussian local frequency estimation. Magn Reson Imaging 2001;19:703–713.
9. Manduca A, Lake DS, Kruse SA, Ehman RL. Spatio-temporal directional filtering for improved inversion of MR elastography images. Med Image Anal 2003;7:465–473.
10. Kruse SA, Smith JA, Lawrence AJ, Dresner MA, Manduca A, Greenleaf JF, Ehman RL. Tissue characterization using magnetic resonance elastography: preliminary results. Phys Med Biol 2000;45:1579–1590.
11. Sack I, Bernarding J, Braun J. Analysis of wave patterns in MR elastography of skeletal muscle using coupled harmonic oscillator simulations. Magn Reson Imaging 2002;20:95–104.
12. Gennisson JL, Catheline S, Chaffai S, Fink M. Transient elastography in anisotropic medium: application to the measurement of slow and fast shear wave speeds in muscles. J Acoust Soc Am 2003;114:536–541.
13. Fedorov FI. Theory of elastic waves in crystals. New York: Plenum; 1968.
14. Musgrave MJP. Crystal acoustics. San Francisco: Holden-Day; 1970.
15. Sjogaard G, Saltin B. Extra- and intracellular water spaces in muscles of man at rest and with dynamic exercise. Am J Physiol 1982;243:R271–R280.
16. Fleckenstein JL, Canby RC, Parkey RW, Peshock RM. Acute effects of exercise on MR imaging of skeletal muscle in normal volunteers. AJR Am J Roentgenol 1988;151:231–237.
17. Saab G, Thompson RT, Marsh GD. Effects of exercise on muscle transverse relaxation determined by MR imaging and in vivo relaxometry. J Appl Physiol 2000;88:226–233.
18. Takeda Y, Kashiwaguchi S, Endo K, Matsuura T, Sasa T. The most effective exercise for strengthening the supraspinatus muscle: evaluation by magnetic resonance imaging. Am J Sports Med 2002;30:374–381.
19. Rump J, Braun J, Papazoglou S, Taupitz M, Sack I. Alterations of the proton-T(2) time in relaxed skeletal muscle induced by passive extremity flexions. J Magn Reson Imaging 2006;23:541–546.
20. Dresner MA, Rose GH, Rossman PJ, Muthupillai R, Manduca A, Ehman RL. Magnetic resonance elastography of skeletal muscle. J Magn Reson Imaging 2001;13:269–276.
21. Jenkyn TR, Ehman RL, An KN. Noninvasive muscle tension measurement using the novel technique of magnetic resonance elastography (MRE). J Biomech 2003;36:1917–1921.
22. Heers G, Jenkyn T, Dresner MA, Klein MO, Basford JR, Kaufman KR, Ehman RL, An KN. Measurement of muscle activity with magnetic resonance elastography. Clin Biomech (Bristol, Avon) 2003;18:537–542.
23. Uffmann K, Maderwald S, Ajaj W, Galban CG, Mateiescu S, Quick HH, Ladd ME. In vivo elasticity measurements of extremity skeletal muscle with MR elastography. NMR Biomed 2004;17:181–190.
24. Papazoglou S, Braun J, Hamhaber U, Sack I. Two-dimensional waveform analysis in MR elastography of skeletal muscles. Phys Med Biol 2005;50:1313–1325.
25. Galban CJ, Maderwald S, Herrmann BL, Brauck K, Grote W, de Greiff A, Uffmann K, Ladd ME. Measuring skeletal muscle elasticity in patients with hypogonadism by MR elastography. In: Proceedings of the 13th Annual Meeting of ISMRM, Miami Beach, FL, USA, 2005. p 2016.
26. Galban CJ, Maderwald S, Eggebrecht H, Grote W, de Greiff A, Uffmann K, Ladd ME. Monitoring the effects of chronic obstructive pulmonary disease on muscle elasticity by MR elastography. In: Proceedings of the 13th Annual Meeting of ISMRM, Miami Beach, FL, USA, 2005. p 2015.
27. Sack I, Samani A, Plewes DB, Braun J. Simulation of in vivo MR elastography wave patterns of skeletal muscles using a transverse isotropic elasticity model. In: Proceedings of the 11th Annual Meeting of ISMRM, Toronto, Canada, 2003. p 587.
28. Every AG, Sachse W. Determination of the elastic constants of anisotropic solids from acoustic-wave group-velocity measurements. Phys Rev B Condens Matter 1990;42:8196–8205.
29. Landau LD, Lifschitz EM. Theory of elasticity. Oxford: Pergamon Press; 1986.
30. Sinkus R, Tanter M, Catheline S, Lorenzen J, Kuhl C, Sondermann E, Fink M. Imaging anisotropic and viscous properties of breast tissue by magnetic resonance-elastography. Magn Reson Med 2005;53:372–387.
31. Sandrin L, Cassereau D, Fink M. The role of the coupling term in transient elastography. J Acoust Soc Am 2004;115:73–83.
32. Rump J, Klatt D, Warmuth C, Braun J, Hamhaber U, Papazoglou S, Sack I. Synchronisation of shear vibrations and balanced steady state free precession in MR elastography (SSFP-MRE). In: Proceedings of the 13th Annual Meeting of ISMRM, Miami Beach, FL, USA, 2005. p 2384.
33. Braun J, Braun K, Sack I. Electromagnetic actuator for generating variably oriented shear waves in MR elastography. Magn Reson Med 2003; 50:220–222.
34. Bernstein MA, King KF, Zhou XJ. Handbook of MRI pulse sequences. Burlington: Elsevier Academic Press; 2004.
35. Kovesi P. Phase congruency: a low-level image invariant. Psychol Res 2000;64:136–148.
36. Bensamoun SF, Ringleb S, Chen Q, Hulshizer T, Rossman P, Ehman RL, An KN. Preliminary database of thigh muscle stiffness using magnetic resonance elastography. In: Proceedings of the 13th Annual Meeting of ISMRM, Miami Beach, FL, USA, 2005. p 2013.
37. Gennisson JL, Cornu C, Catheline S, Fink M, Portero P. Human muscle hardness assessment during incremental isometric contraction using transient elastography. J Biomech 2005;38:1543–1550.
38. Oida T, Kang Y, Azuma T, Okamoto J, Amano A, Axel L, Takizawa O, Tsutsumi S, Matsuda T. The measurement of anisotropic elasticity in skeletal muscle using MR elastography. In: Proceedings of the 13th Annual Meeting of ISMRM, Miami Beach, FL, USA, 2005. p 2020.
39. Barbone PE, Gokhale NH. Elastic modulus imaging: on the uniqueness and nonuniqueness of the elastography inverse problem in two dimensions. Inverse Probl 2004;20:283–296.